10.1071/CH09467_AC

Australian Journal of Chemistry, 2010, 63(4), 687–692

Accessory Publication

Supramolecular Chemistry of Pyronines B and Y, β-Cyclodextrin and Linked β-Cyclodextrins

Huy T. Ngo,[A] *Philip Clements*,[A] *Christopher J. Easton*,[B] *Duc-Truc Pham*,[A] and *Stephen F. Lincoln*[A,C]

[A]School of Chemistry and Physics, University of Adelaide, South Australia 5005, Australia.

[B]Research School of Chemistry, Australian National University, Canberra, ACT 0200, Australia.

[C]Corresponding author. Tel: +61 8 8303 5559.

Fax: +61 8 8303 4358.

Email: stephen.lincoln@adelaide.edu.au

Sequence

UV-Vis and Fluorescence Titrations and Fitting (Figs. A1 – A24)
^{1}H NMR Titrations and Fittings (Figs. A25 – A62)
2D NOESY ^{1}H NMR Spectra (Figs. A63 – A66)

^{1}H NMR Chemical Shift Data (Table A1)

UV-Vis and Fluorescence Titrations and Fitting (Figs. A1 – A24)

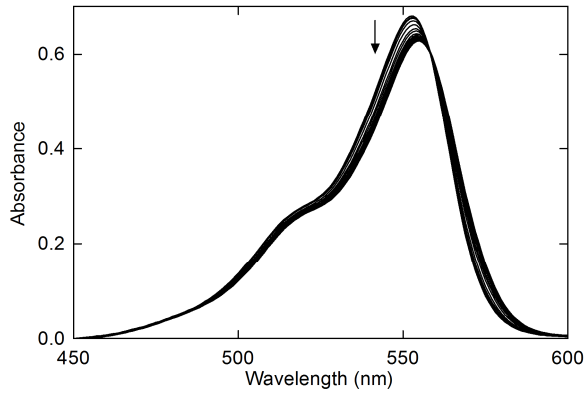

Fig. A1. UV-visible absorbance spectra of PB^+ alone (6.35×10^{-6} mol dm^{-3}) and in the presence of increasing concentrations of βCD (ranging from 0.00 to 6.50×10^{-3} mol dm^{-3}) in aqueous hydrochloric acid (1.00×10^{-4} mol dm^{-3}, I = 0.10 mol dm^{-3} NaCl) at 298.2 K. The arrow indicates the direction of absorbance change as $[\beta CD]_{total}$ increases. An isosbestic point occurs at 558 nm. λ_{max} = 553 nm ($\varepsilon = 1.07 \times 10^5$ dm^3 mol^{-1} cm^{-1}) and 555 nm ($\varepsilon = 9.82 \times 10^4$ dm^3 mol^{-1} cm^{-1}) for the free and complexed PB^+ species, respectively.

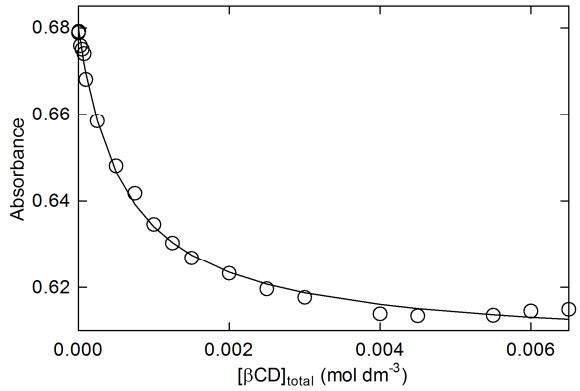

Fig. A2. UV-visible absorbance variation of PB^+ (6.35×10^{-6} mol dm^{-3}) with βCD (0.00 to 6.50×10^{-3} mol dm^{-3}) in aqueous hydrochloric acid (1.00×10^{-4} mol dm^{-3}, I = 0.10 mol dm^{-3} NaCl) at 298.2 K. The circles represent experimental data at 552 nm and the solid line represents the best fit of an equation analogous to eqn. 4 in the main text for a 1:1 complexation model in the range 500-590 nm.

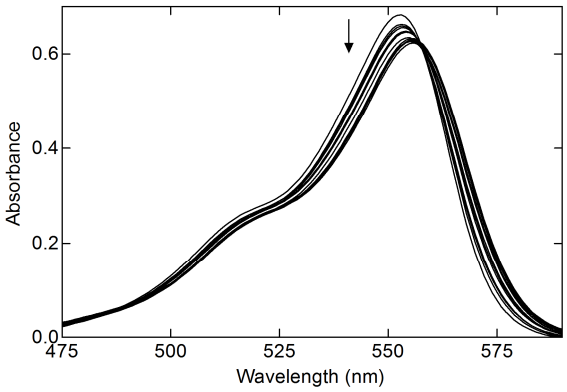

Fig. A3. UV-visible absorbance spectra of PB^+ alone (6.38×10^{-6} mol dm^{-3}) and in the presence of increasing concentrations of 66βCD$_2$suc (ranging from 0.00 to 2.01×10^{-3} mol dm^{-3}) in aqueous hydrochloric acid (1.00×10^{-4} mol dm^{-3}, I = 0.10 mol dm^{-3} NaCl) at 298.2 K. The arrow indicates the direction of absorbance change as $[66\beta CD_2suc]_{total}$ increases. An isosbestic point occurs at 558 nm. λ_{max} = 553 nm ($\varepsilon = 1.07 \times 10^5$ dm^3 mol^{-1} cm^{-1}) and 556 nm ($\varepsilon = 9.83 \times 10^4$ dm^3 mol^{-1} cm^{-1}) for the free and complexed PB^+ species, respectively.

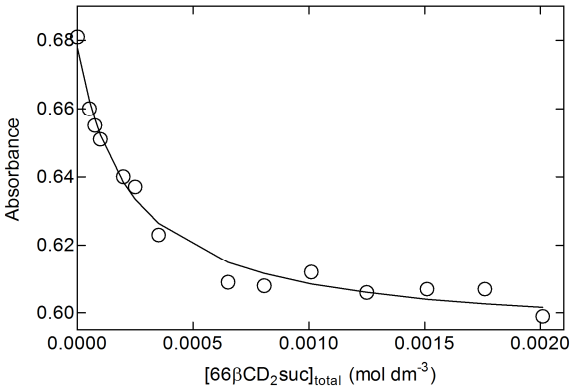

Fig. A4. UV-visible absorbance variation of PB^+ (6.38×10^{-6} mol dm^{-3}) with 66βCD$_2$suc (0.00 to 2.01×10^{-3} mol dm^{-3}) in aqueous hydrochloric acid (1.00×10^{-4} mol dm^{-3}, I = 0.10 mol dm^{-3} NaCl) at 298.2 K. The circles represent experimental data at 552 nm and the solid line represents the best fit of an equation analogous to eqn. 4 in the main text for a 1:1 complexation model in the range 500-590 nm.

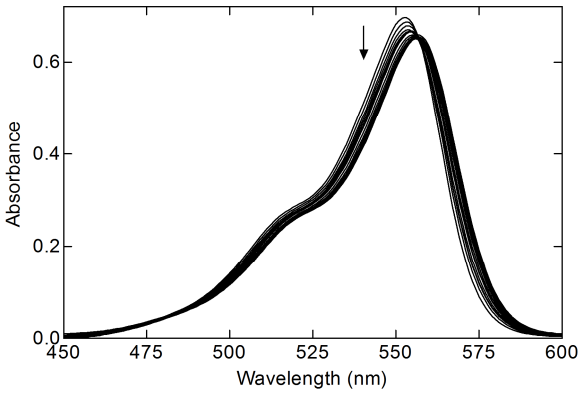

Fig. A5. UV-visible absorbance spectra of PB^+ alone (6.51×10^{-6} mol dm^{-3}) and in the presence of increasing concentrations of 33βCD$_2$suc (ranging from 0.00 to 1.97×10^{-3} mol dm^{-3}) in aqueous hydrochloric acid (1.00×10^{-4} mol dm^{-3}, I = 0.10 mol dm^{-3} NaCl) at 298.2 K. The arrow indicates the direction of absorbance change as $[33\beta CD_2suc]_{total}$ increases. An isosbestic point occurs at 556 nm. λ_{max} = 553 nm ($\varepsilon = 1.07 \times 10^5$ dm^3 mol^{-1} cm^{-1}) and 557 nm ($\varepsilon = 1.01 \times 10^5$ dm^3 mol^{-1} cm^{-1}) for the free and complexed PB^+ species, respectively.

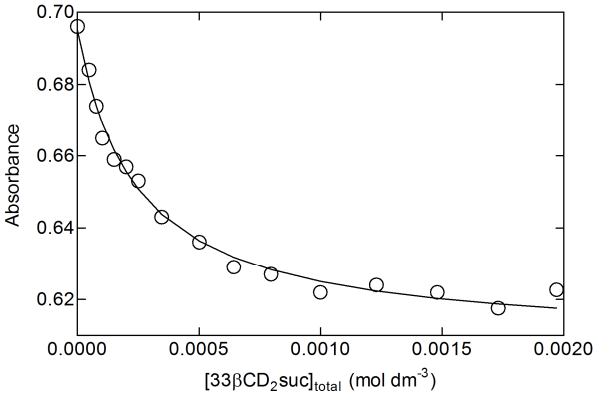

Fig. A6. UV-visible absorbance variation of PB^+ (6.51×10^{-6} mol dm^{-3}) with 33βCD$_2$suc (0.00 to 1.97×10^{-3} mol dm^{-3}) in aqueous ydrochloric acid (1.00×10^{-4} mol dm^{-3}, I = 0.10 mol dm^{-3} NaCl) at 298.2 K. The circles represent experimental data at 552 nm and the solid line represents represents the best fit of an equation analogous to eqn. 4 in the main text for a 1:1 complexation model in the range 500-590 nm.

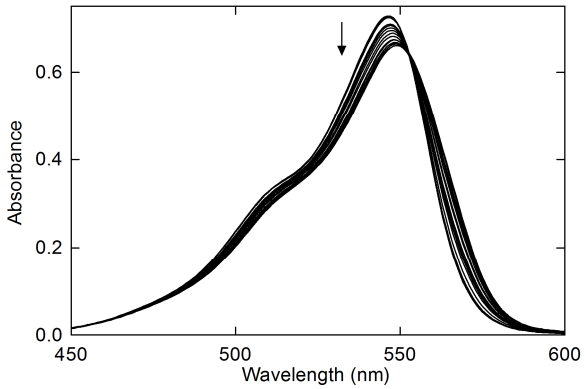

Fig. A7. UV-visible absorbance spectra of PY^+ alone (8.99×10^{-6} mol dm^{-3}) and in the presence of increasing concentrations of βCD (ranging from 0.00 to 9.37×10^{-3} mol dm^{-3}) in aqueous hydrochloric acid (1.00×10^{-4} mol dm^{-3}, I = 0.10 mol dm^{-3} NaCl) at 298.2 K. The arrow indicates the direction of absorbance change as $[\beta CD]_{total}$ increases. An isosbestic point occurs at 553 nm. λ_{max} = 546 nm ($\varepsilon = 8.10 \times 10^4$ dm^3 mol^{-1} cm^{-1}) and 550 nm ($\varepsilon = 7.19 \times 10^4$ dm^3 mol^{-1} cm^{-1}) for the free and complexed PY^+ species, respectively.

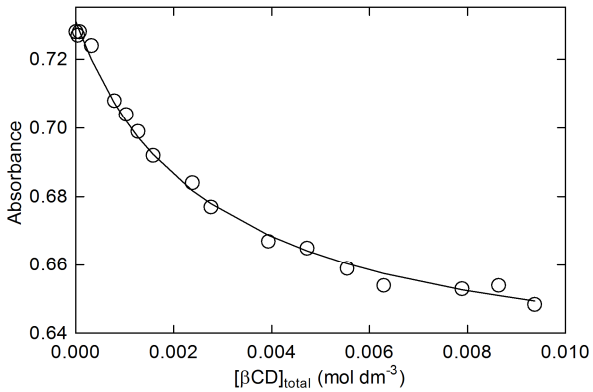

Fig. A8. UV-visible absorbance variation of PY^+ (8.99×10^{-6} mol dm^{-3}) with βCD (0.00 to 9.37×10^{-3} mol dm^{-3}) in aqueous hydrochloric acid (1.00×10^{-4} mol dm^{-3}, I = 0.10 mol dm^{-3} NaCl) at 298.2 K. The circles represent experimental data at 546 nm and the solid line represents the best fit of an equation analogous to eqn. 4 in the main text for a 1:1 complexation model in the range 500-590 nm.

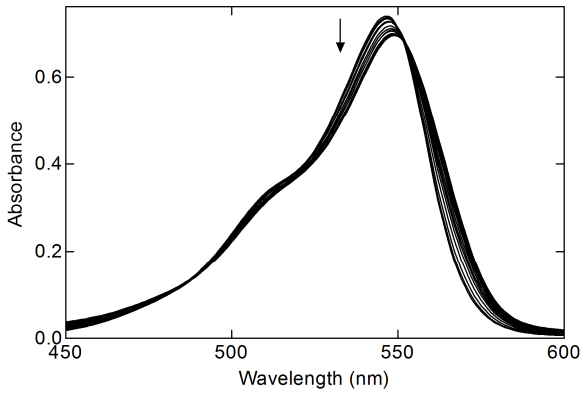

Fig. A9. UV-visible absorbance spectra of PY^+ alone (9.18×10^{-6} mol dm^{-3}) and in the presence of increasing concentrations of 66βCD$_2$suc (ranging from 0.00 to 2.74×10^{-3} mol dm^{-3}) in aqueous hydrochloric acid (1.00×10^{-4} mol dm^{-3}, I = 0.10 mol dm^{-3} NaCl) at 298.2 K. The arrow indicates the direction of absorbance change as $[66\beta CD_2suc]_{total}$ increases. An isosbestic point occurs at 552 nm. λ_{max} = 546 nm ($\varepsilon = 8.10 \times 10^4$ dm^3 mol^{-1} cm^{-1}) and 551 nm ($\varepsilon = 7.46 \times 10^4$ dm^3 mol^{-1} cm^{-1}) for the free and complexed PY^+ species, respectively.

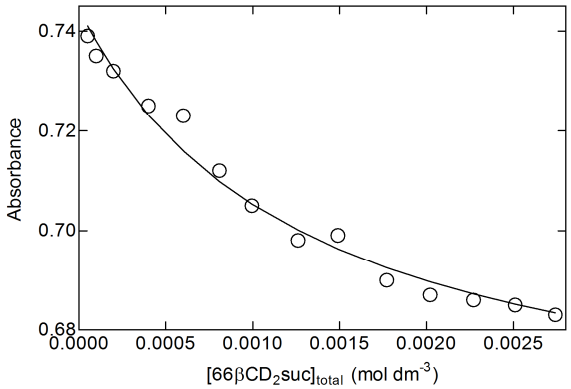

Fig. A10. UV-visible absorbance variation of PY^+ (9.18×10^{-6} mol dm^{-3}) with 66βCD$_2$suc (0.00 to 2. 74×10^{-3} mol dm^{-3}) in aqueous hydrochloric acid (1.00×10^{-4} mol dm^{-3}, I = 0.10 mol dm^{-3} NaCl) at 298.2 K. The circles represent experimental data at 546 nm and the solid line represents the best fit of an equation analogous to eqn. 4 in the main text in the range 500-590 nm.

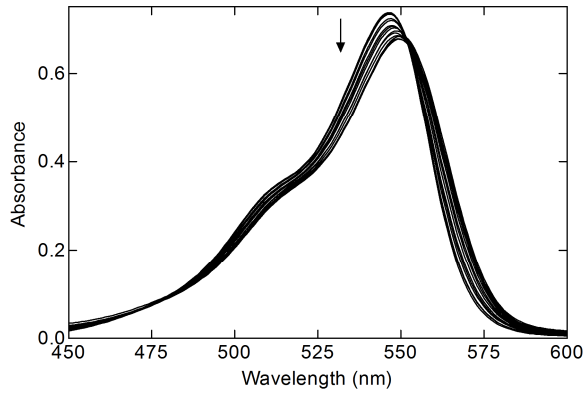

Fig. A11. UV-visible absorbance spectra of PY^+ alone (9.10×10^{-6} mol dm^{-3}) and in the presence of increasing concentrations of 33βCD_2suc (ranging from 0.00 to 2.50×10^{-3} mol dm^{-3}) in aqueous hydrochloric acid (1.00×10^{-4} mol dm^{-3}, I = 0.10 mol dm^{-3} NaCl) at 298.2 K. The arrow indicates the direction of absorbance change as $[33\beta CD_2suc]_{total}$ increases. An isosbestic point occurs at 552 nm. λ_{max} = 546 nm ($\varepsilon = 8.10 \times 10^4$ dm^3 mol^{-1} cm^{-1}) and 553 nm ($\varepsilon = 7.41 \times 10^4$ dm^3 mol^{-1} cm^{-1}) for the free and complexed PY^+ species, respectively.

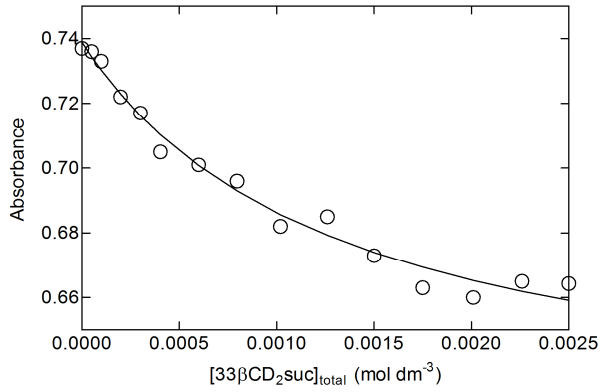

Fig. A12. UV-visible absorbance variation of PY^+ (9.10×10^{-6} mol dm^{-3}) with 33βCD_2suc (0.00 to 2. 50×10^{-3} mol dm^{-3}) in aqueous hydrochloric acid (1.00×10^{-4} mol dm^{-3}, I = 0.10 mol dm^{-3} NaCl) at 298.2 K. The circles represent experimental data at 546 nm and the solid line represents the best fit of an equation analogous to eqn. 4 in the main text for a 1:1 complexation model in the range 500-590 nm.

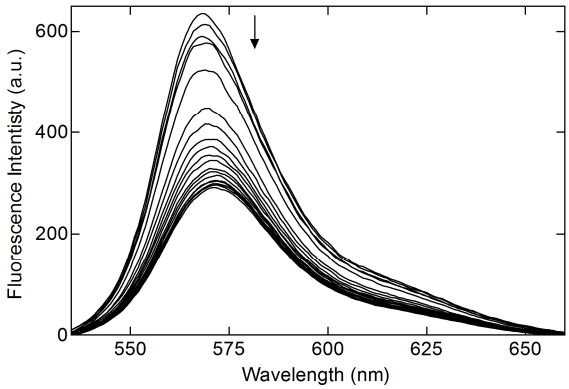

Fig. A13. Emission spectra of PB^+ alone (6.02×10^{-7} mol dm^{-3}) and in the presence of increasing concentrations of βCD (ranging from 0.00 to 7.00×10^{-3} mol dm^{-3}) in aqueous hydrochloric acid (1.00×10^{-4} mol dm^{-3}, I = 0.10 mol dm^{-3} NaCl) at 298.2 K. Excitation wavelength λ_{ex} = 515 nm with excitation and emission slit widths of 5 nm. The arrow indicates the direction of relative fluorescence emission change as $[\beta CD]_{total}$ increases. λ_{max} = 568 nm (641 a.u.) and 572 nm (269 a.u.) for the free and complexed PB^+ species, respectively.

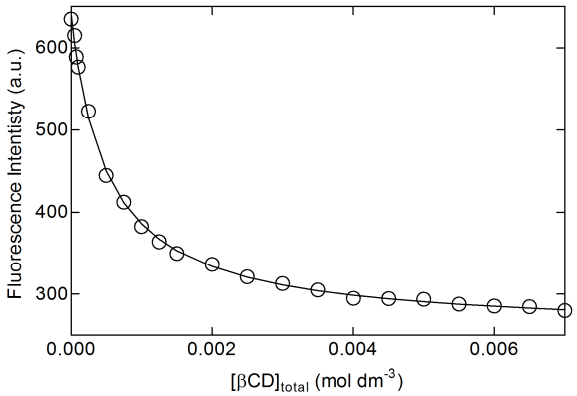

Fig. A14. Relative fluorescence variation of PB^+ (6.02×10^{-7} mol dm^{-3}) with βCD (0.00 to 7.00×10^{-3} mol dm^{-3}) in aqueous hydrochloric acid (1.00×10^{-4} mol dm^{-3}, I = 0.10 mol dm^{-3} NaCl) at 298.2 K. Emission was measured at 568 nm. The circles represent experimental data and the solid line represents the best fit of an equation analogous to eqn. 4 in the main text for a 1:1 complexation model in the range 540-650 nm.

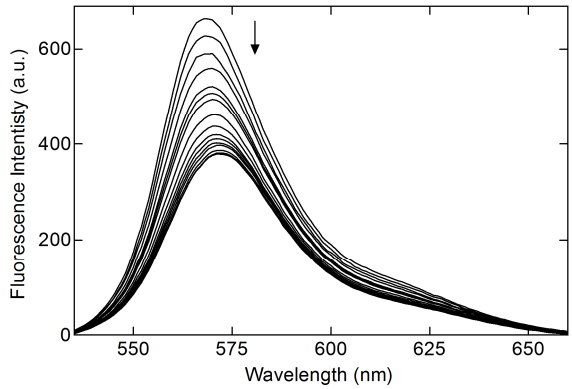

Fig. A15. Emission spectra of PB^+ alone (6.28×10^{-7} mol dm^{-3}) and in the presence of increasing concentrations of 66βCD$_2$suc (ranging from 0.00 to 1.97×10^{-3} mol dm^{-3}) in aqueous hydrochloric acid (1.00×10^{-4} mol dm^{-3}, I = 0.10 mol dm^{-3} NaCl) at 298.2 K. Excitation wavelength λ_{ex} = 515 nm with excitation and emission slit widths of 5 nm. The arrow indicates the direction of relative fluorescence emission change as $[66\beta CD_2suc]_{total}$ increases. λ_{max} = 568 nm (662 a.u.) and 572 nm (354 a.u.) for the free and complexed PB^+ species, respectively.

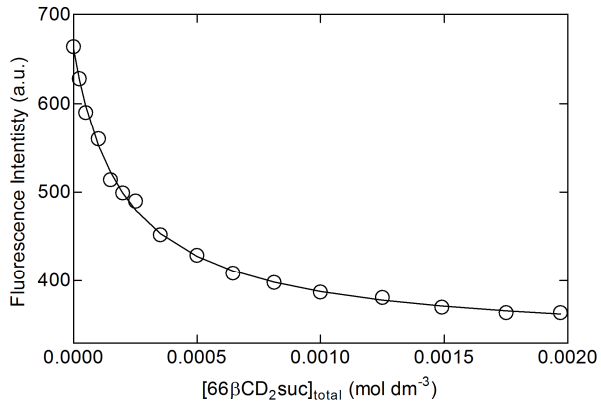

Fig. A16. Relative fluorescence variation of PB^+ (6.28×10^{-7} mol dm^{-3}) with 66βCD$_2$suc (0.00 to 1.97×10^{-3} mol dm^{-3}) in aqueous hydrochloric acid (1.00×10^{-4} mol dm^{-3}, I = 0.10 mol dm^{-3} NaCl) at 298.2 K. Emission was measured at 568 nm. The circles represent experimental data and the solid line represents the best fit of an equation analogous to eqn. 4 in the main text for a 1:1 complexation model in the range 540-650 nm.

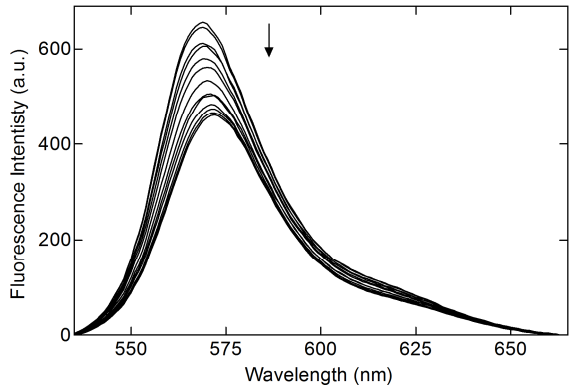

Fig. A17. Emission spectra of PB^+ alone (6.19×10^{-7} mol dm^{-3}) and in the presence of increasing concentrations of $33\beta CD_2suc$ (ranging from 0.00 to 1.54×10^{-3} mol dm^{-3}) in aqueous hydrochloric acid (1.00×10^{-4} mol dm^{-3}, I = 0.10 mol dm^{-3} NaCl) at 298.2 K. Excitation wavelength λ_{ex} = 515 nm with excitation and emission slit widths of 5 nm. The arrow indicates the direction of relative fluorescence emission change as $[33\beta CD_2suc]_{total}$ increases. λ_{max} = 568 nm (656 a.u.) and 572 nm (431 a.u.) for the free and complexed PB^+ species, respectively.

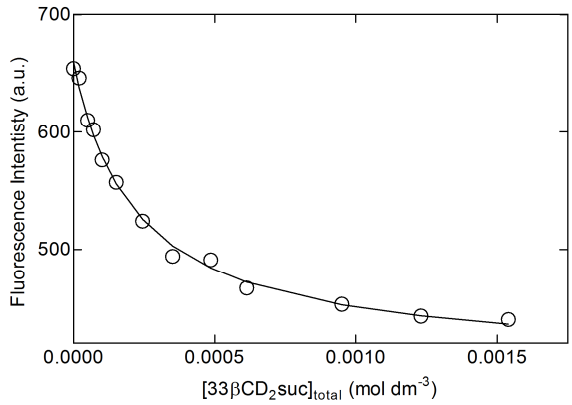

Fig. A18. Relative fluorescence variation of PB^+ (6.19×10^{-7} mol dm^{-3}) with $33\beta CD_2suc$ (0.00 to 1.54×10^{-3} mol dm^{-3}) in aqueous hydrochloric acid (1.00×10^{-4} mol dm^{-3}, I = 0.10 mol dm^{-3} NaCl) at 298.2 K. Emission was measured at 568 nm. The circles represent experimental data and the solid line represents the best fit of an equation analogous to eqn. 4 in the main text for a 1:1 complexation model in the range 540-650 nm.

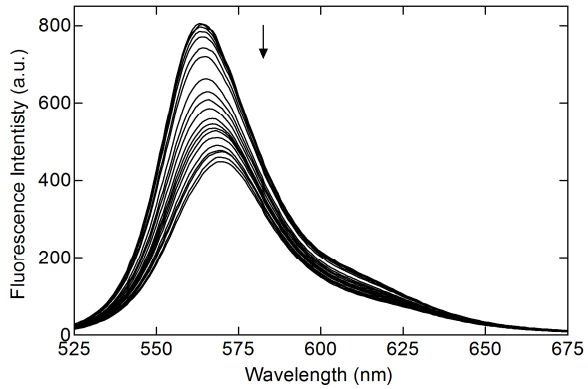

Fig. A19. Emission spectra of PY^+ alone (9.19×10^{-7} mol dm^{-3}) and in the presence of increasing concentrations of βCD (ranging from 0.00 to 9.65×10^{-3} mol dm^{-3}) in aqueous hydrochloric acid (1.00×10^{-4} mol dm^{-3}, I = 0.10 mol dm^{-3} NaCl) at 298.2 K. Excitation wavelength λ_{ex} = 500 nm with excitation and emission slit widths of 5 nm. The arrow indicates the direction of relative fluorescence emission change as $[\beta CD]_{total}$ increases. λ_{max} = 563 nm (816.5 a.u.) and 572 nm (365 a.u.) for the free and complexed PY^+ species, respectively.

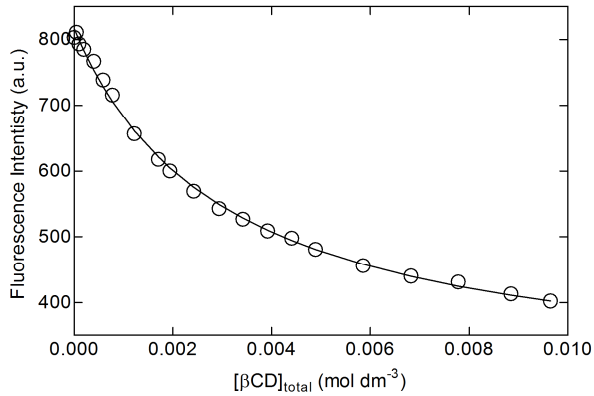

Fig. A20. Relative fluorescence variation of PY^+ (9.19×10^{-7} mol dm^{-3}) with βCD (0.00 to 9.65×10^{-3} mol dm^{-3}) in aqueous hydrochloric acid (1.00×10^{-4} mol dm^{-3}, I = 0.10 mol dm^{-3} NaCl) at 298.2 K. Emission was measured at 563 nm. The circles represent experimental data and the solid line represents the best fit of an equation analogous to eqn. 4 in the main text for a 1:1 complexation model in the range 530-630 nm.

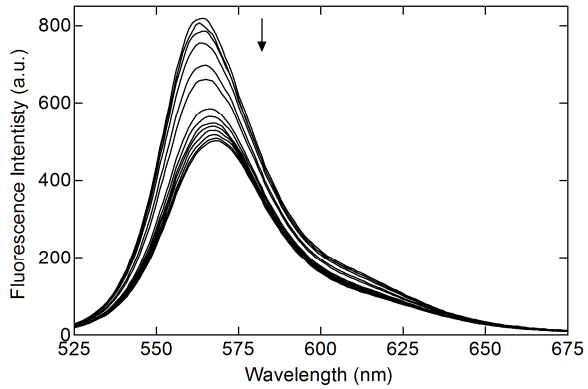

Fig. A21. Emission spectra of PY^+ alone (9.62×10^{-7} mol dm^{-3}) and in the presence of increasing concentrations of 66βCD$_2$suc (ranging from 0.00 to 2.59×10^{-3} mol dm^{-3}) in aqueous hydrochloric acid (1.00×10^{-4} mol dm^{-3}, I = 0.10 mol dm^{-3} NaCl) at 298.2 K. Excitation wavelength λ_{ex} = 500 nm with excitation and emission slit widths of 5 nm. The arrow indicates the direction of relative fluorescence emission change as $[66\beta CD_2suc]_{total}$ increases. λ_{max} = 563 nm (820 a.u.) and 572 nm (375 a.u.) for the free and complexed PY^+ species, respectively.

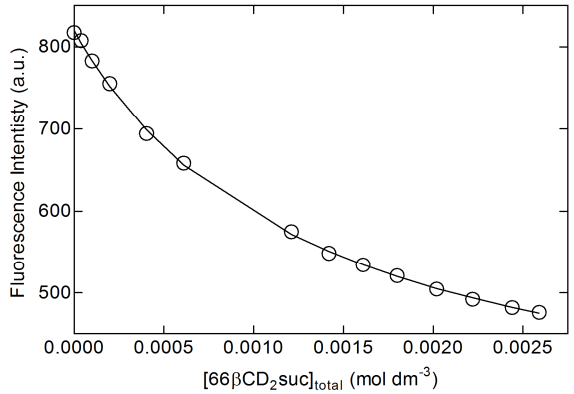

Fig. A22. Relative fluorescence variation of PY^+ (9.62×10^{-7} mol dm^{-3}) with 66βCD$_2$suc (0.00 to 2.59×10^{-3} mol dm^{-3}) in aqueous hydrochloric acid (1.00×10^{-4} mol dm^{-3}, I = 0.10 mol dm^{-3} NaCl) at 298.2 K. Emission was measured at 563 nm. The circles represent experimental data and the solid line represents the best fit of an equation analogous to eqn. 4 in the main text for a 1:1 complexation model in the range 530-630 nm.

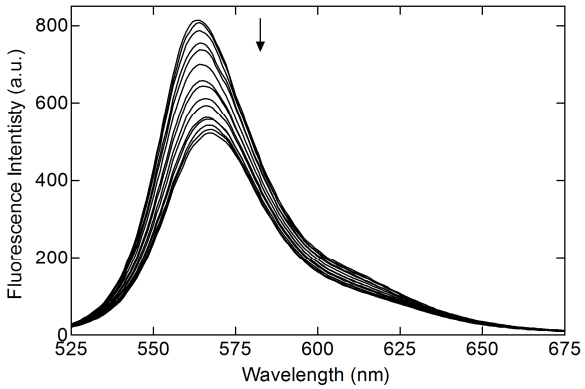

Fig. A23. Emission spectra of PY^+ alone (9.56×10^{-7} mol dm^{-3}) and in the presence of increasing concentrations of 33βCD$_2$suc (ranging from 0.00 to 2.49×10^{-3} mol dm^{-3}) in aqueous hydrochloric acid (1.00×10^{-4} mol dm^{-3}, I = 0.10 mol dm^{-3} NaCl) at 298.2 K. Excitation wavelength λ_{ex} = 500 nm with excitation and emission slit widths of 5 nm. The arrow indicates the direction of relative fluorescence emission change as $[33\beta CD_2suc]_{total}$ increases. λ_{max} = 563 nm (819 a.u.) and 572 nm (400 a.u.) for the free and complexed PY^+ species, respectively.

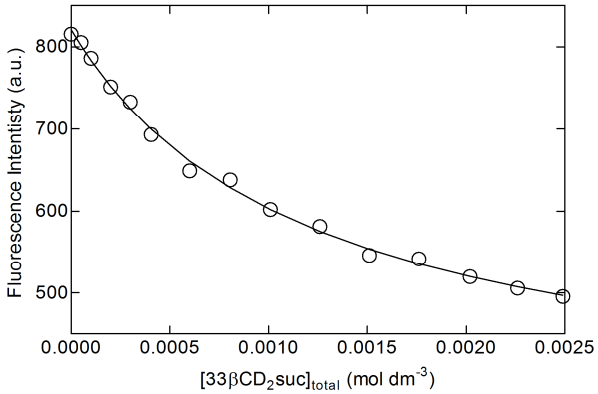

Fig. A24. Relative fluorescence variation of PY^+ (9.56×10^{-7} mol dm^{-3}) with 33βCD$_2$suc (0.00 to 2.49×10^{-3} mol dm^{-3}) in aqueous hydrochloric acid (1.00×10^{-4} mol dm^{-3}, I = 0.10 mol dm^{-3} NaCl) at 298.2 K. Emission was measured at 563 nm. The circles represent experimental data and the solid line represents the best fit of an equation analogous to eqn. 4 in the main text for a 1:1 complexation model in the range 530-630 nm.

^{1}H NMR Titrations and Fittings

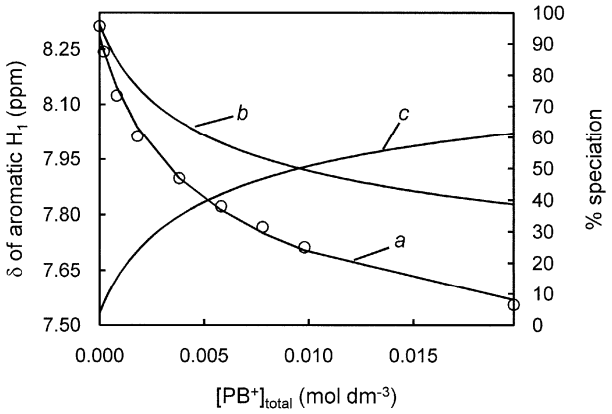

Fig. A25

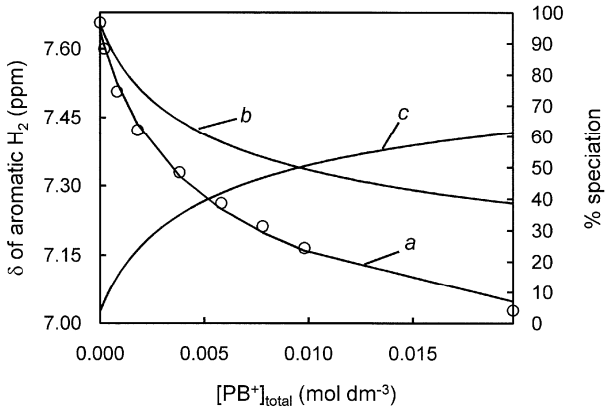

Fig. A26

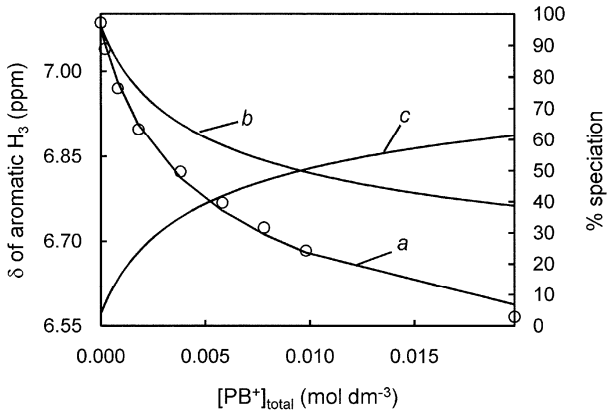

Fig. A27

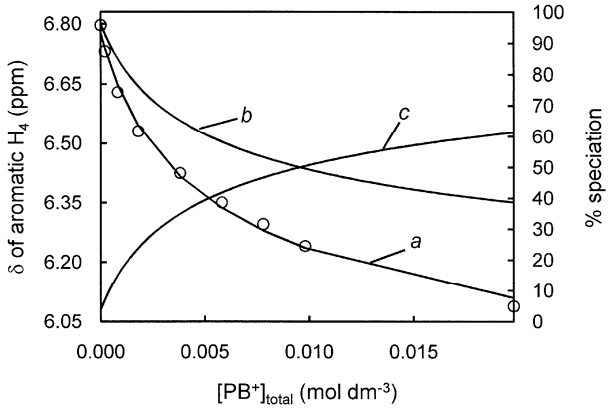

Fig. A28

Collective Caption for Figs. A25-A28. Left ordinate: variation of the ^{1}H (300 MHz) chemical shift of the aromatic H_1 proton (**Fig. A25**), aromatic H_2 proton (**Fig. A26**), aromatic H_3 proton (**Fig. A27**) and aromatic H_4 proton (**Fig. A28**) of PB^+ with $[PB^+]_{total}$ (ranging from 2.00×10^{-4} mol dm^{-3} to 2.00×10^{-2} mol dm^{-3}) in D_2O (1.00×10^{-4} mol dm^{-3} hydrochloric acid, I = 0.10 mol dm^{-3} NaCl) at 298.2 K. The circles are the experimental data and the solid curve *a* is the best fit of the algorithm for dimezisation of PB^+ to the chemical shift variations of protons H_1-H_4. Right ordinate: speciation relative to $[PB^+]_{total}$, curve *b* is the percentage of $[PB^+]$ and curve *c* is twice the percentage of $[(PB^+)_2]$.

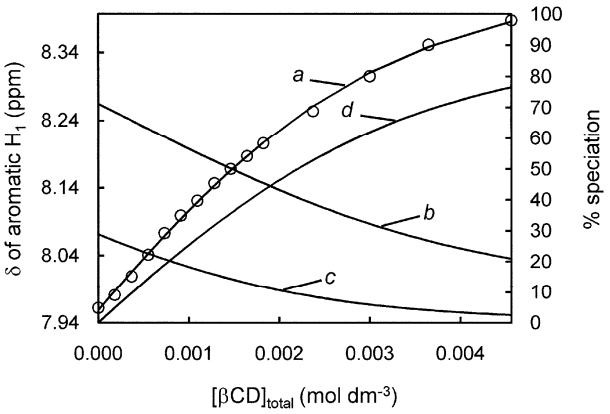

Fig. A29

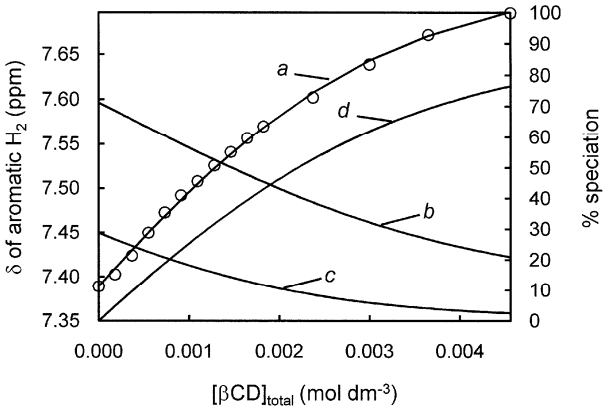

Fig. A30

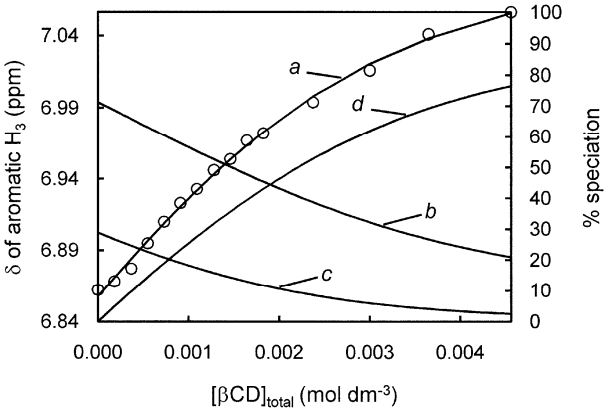

Fig. A31

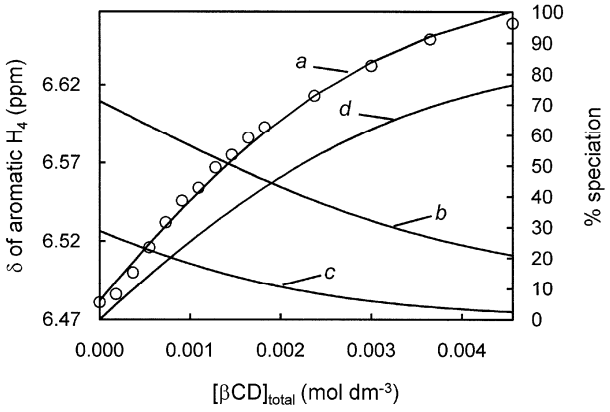

Fig. A32

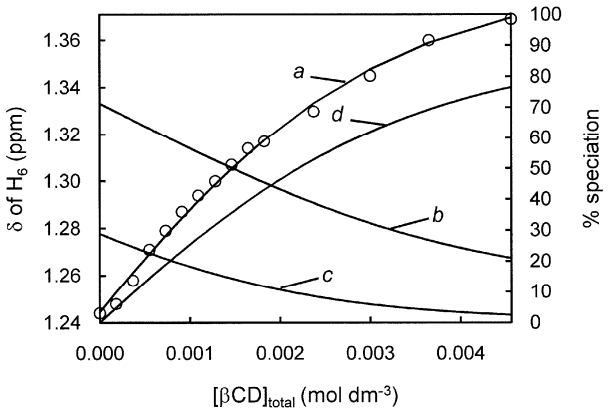

Fig. A33

Collective Caption for Figs. A29-A33. Left ordinate: variation of the ^{1}H (300 MHz) chemical shift of the aromatic H_1 proton (**Collective Caption for A29**), aromatic H_2 proton (**Fig. A30**), aromatic H_3 proton (**Fig. A31**), aromatic H_4 proton (**Collective Caption for A33**) and H_6 proton (**Fig. A33**) of PB^+ (2.75×10^{-3} mol dm^{-3}) with $[\beta CD]_{total}$ (ranging from 0 to 4.60×10^{-3} mol dm^{-3}) in D_2O (1.00×10^{-4} mol dm^{-3} hydrochloric acid, I = 0.10 mol dm^{-3} NaCl) at 298.2 K. The circles are the experimental data and the solid curve *a* is the best fit of the algorithm incorporating PB^+, $(PB^+)_2$ and $\beta CD.PB^+$ to the chemical shift variations of protons H_1-H_4 and H_6. Right ordinate: speciation relative to $[PB^+]_{total}$, curve *b* is the percentage of $[PB^+]$, curve *c* is 2 × the percentage of $[(PB^+)_2]$ and curve *d* is the percentage of $[\beta CD.PB^+]$.

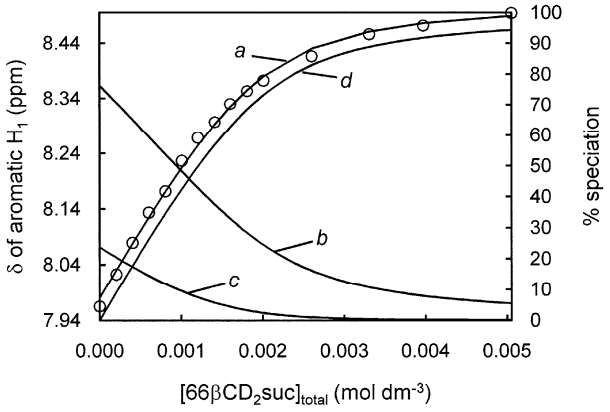

Fig. A34

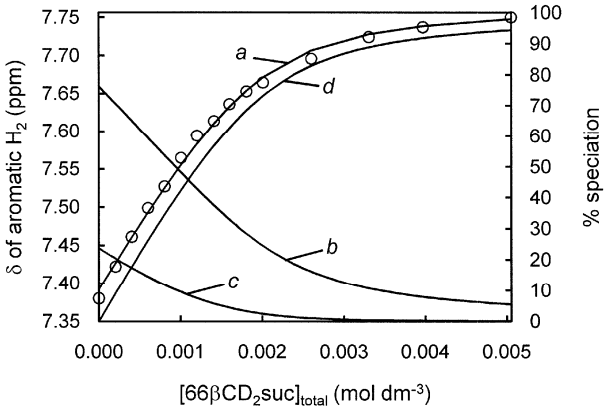

Fig. A35

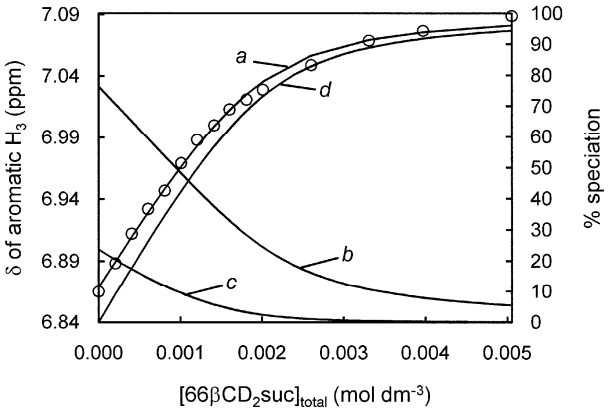

Fig. A36

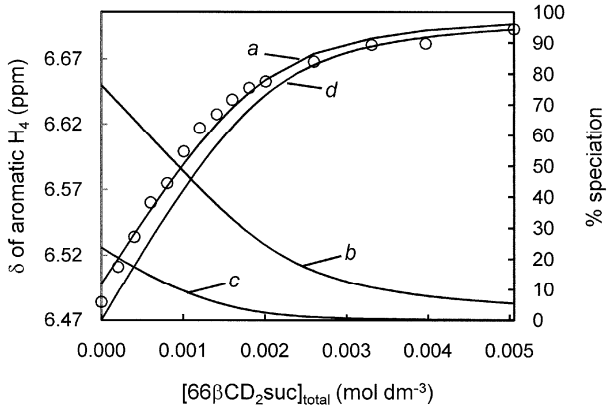

Fig. A37

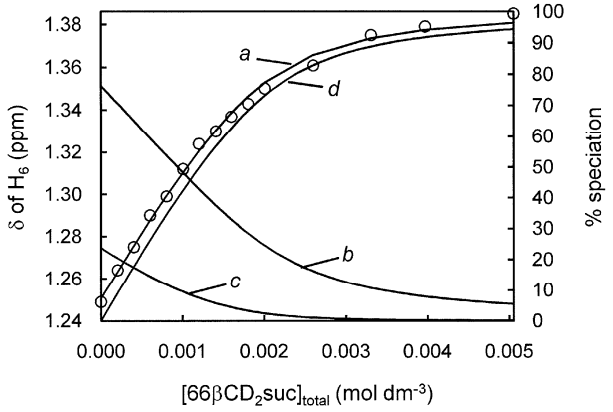

Fig. A38

Collective Caption for Figs. A34-A38. Left ordinate: variation of the ^{1}H (300 MHz) chemical shift of the aromatic H_1 proton (**Fig. A34**), aromatic H_2 proton (**Fig. A35**), aromatic H_3 proton (**Fig. A36**), aromatic H_4 proton (**Fig. A37**) and H_6 proton (**Fig. A38**) of PB^+ (2.00×10^{-3} mol dm^{-3}) with $[66\beta CD_2suc]_{total}$ (ranging from 0 to 5.00×10^{-3} mol dm^{-3}) in D_2O (1.00×10^{-4} mol dm^{-3} hydrochloric acid, I = 0.10 mol dm^{-3} NaCl) at 298.2 K. The circles are the experimental data and the solid curve *a* is the best fit of the algorithm incorporating PB^+, $(PB^+)_2$ and $66\beta CD_2suc.PB^+$ to the chemical shift variations of protons H_1-H_4 and H_6. Right ordinate: speciation relative to $[PB^+]_{total}$, curve *b* is the percentage of $[PB^+]$, curve *c* is twice the percentage of $[(PB^+)_2]$ and curve *d* is the percentage of $[66\beta CD_2suc.PB^+]$.

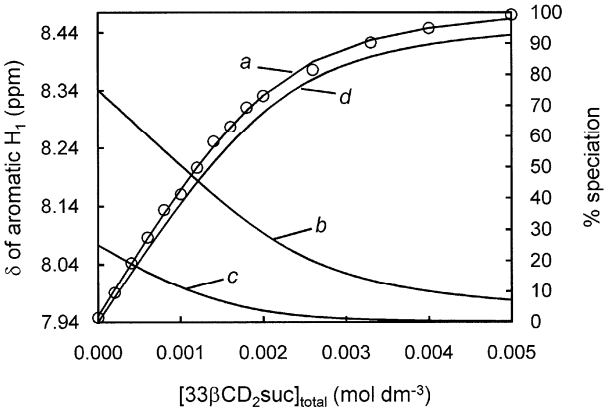

Fig. A39

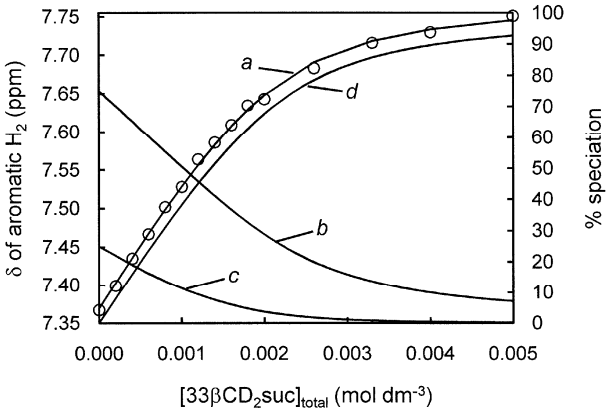

Fig. A40

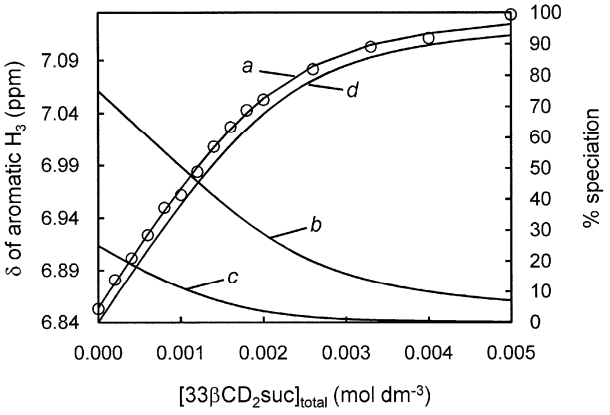

Fig. A41

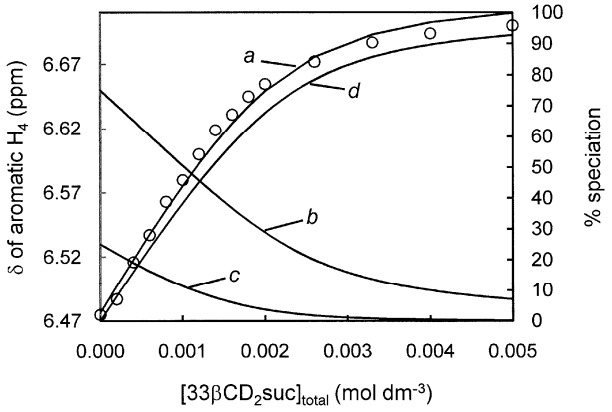

Fig. A42

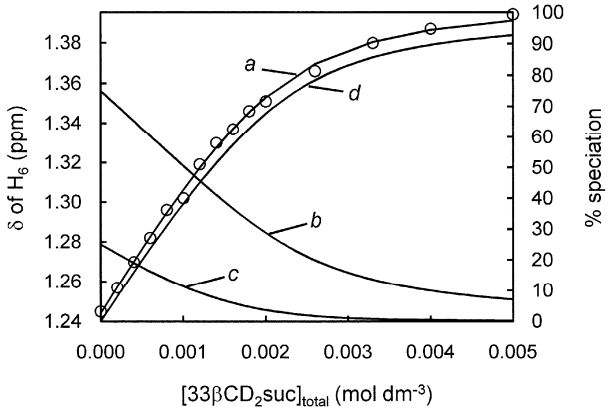

Fig. A43

Collective Caption for Figs. A38-A43. Left ordinate: variation of the ^{1}H (300 MHz) chemical shift of the aromatic H_1 proton (**Fig. A39**), aromatic H_2 proton (**Fig. A40**), aromatic H_3 proton (**Fig. A41**), aromatic H_4 proton (**Fig. A42**) and H_6 proton (**Fig. A43**) of PB^+ (2.15×10^{-3} mol dm^{-3}) with $[33\beta CD_2suc]_{total}$ (ranging from 0 to 5.00×10^{-3} mol dm^{-3}) in D_2O (1.00×10^{-4} mol dm^{-3} hydrochloric acid, I = 0.10 mol dm^{-3} NaCl) at 298.2 K. The circles are the experimental data and the solid curve *a* is the best fit of the algorithm incorporating PB^+, $(PB^+)_2$ and $33\beta CD_2suc.PB^+$ to the chemical shift variations of protons H_1-H_4 and H_6. Right ordinate: speciation relative to $[PB^+]_{total}$, curve *b* is the percentage of $[PB^+]$, curve *c* is twice the percentage of $[(PB^+)_2]$ and curve *d* is the percentage of $[33\beta CD_2suc.PB^+]$.

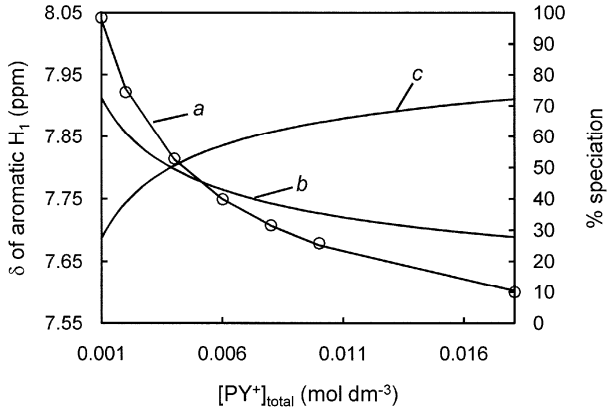

Fig. A44

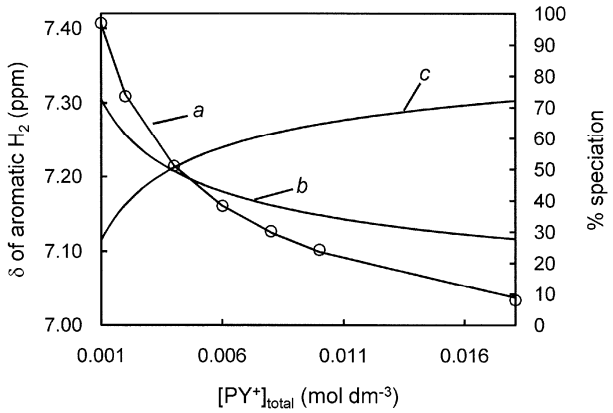

Fig. A45

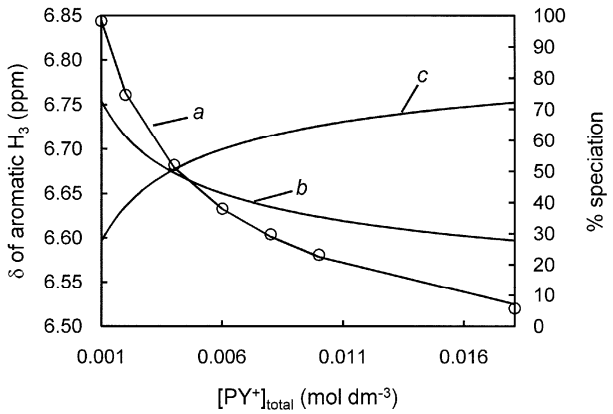

Fig. A46

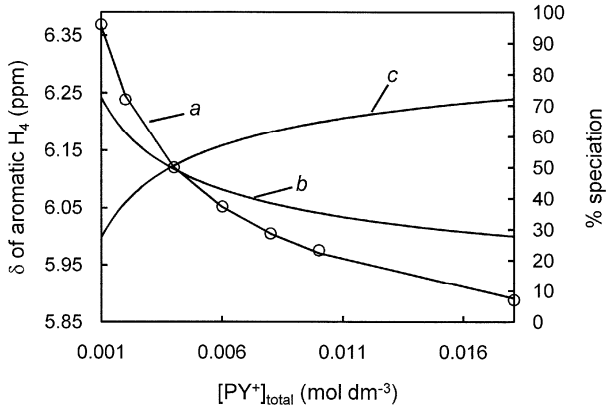

Fig. A47

Collective Caption for Figs. A44-A47. Left ordinate: variation of the ^{1}H (300 MHz) chemical shift of the aromatic H_1 proton (**Fig. A44**), aromatic H_2 proton (**Fig. A45**), aromatic H_3 proton (**Fig. A46**) and aromatic H_4 proton (**Fig. A47**) of PY^+ with $[PY^+]_{total}$ (ranging from 2.00×10^{-3} mol dm^{-3} to 1.81×10^{-2} mol dm^{-3}) in D_2O (1.00×10^{-4} mol dm^{-3} hydrochloric acid, I = 0.10 mol dm^{-3} NaCl) at 298.2 K. The circles are the experimental data and the solid curve *a* is the best fit of the algorithm for dimerisation of PY^+ to the chemical shift variations of protons H_1-H_4. Right ordinate: speciation relative to $[PY^+]_{total}$, curve *b* is the percentage of $[PY^+]$ and curve *c* is twice the percentage of $[(PY^+)_2]$.

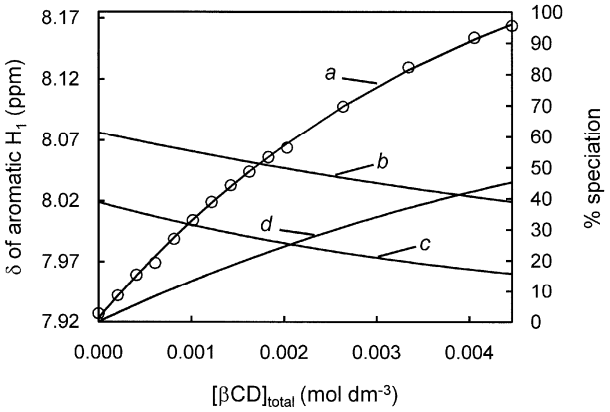

Fig. A48

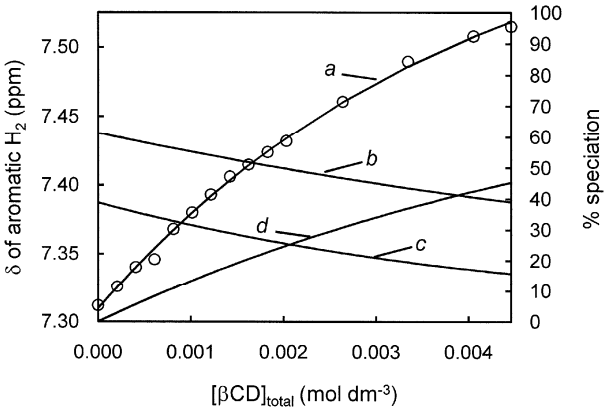

Fig. A49

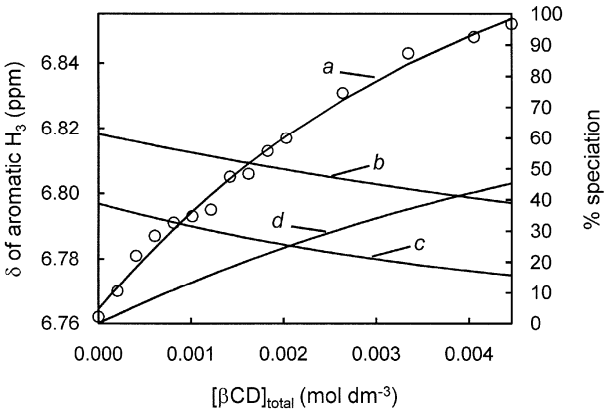

Fig. A50

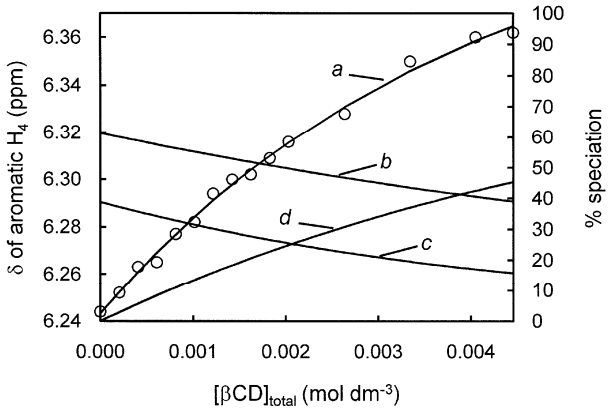

Fig. A51

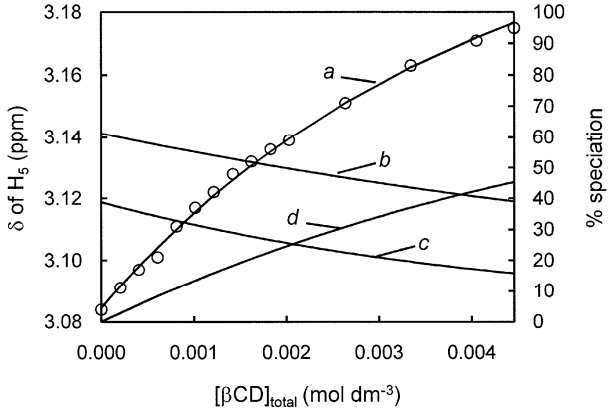

Fig. A52

Collective Caption for Figs. A48-A52. Left ordinate: variation of the ^{1}H (300 MHz) chemical shift of the aromatic H_1 proton (**Fig. A48**), aromatic H_2 proton (**Fig. A49**), aromatic H_3 proton (**Fig. A50**), aromatic H_4 proton (**Fig. A51**) and H_5 proton (**Fig. A52**) of PY^+ (2.00×10^{-3} mol dm^{-3}) with $[\beta CD]_{total}$ (ranging from 0 to 4.50×10^{-3} mol dm^{-3}) in D_2O (1.00×10^{-4} mol dm^{-3} hydrochloric acid, I = 0.10 mol dm^{-3} NaCl) at 298.2 K. The circles are the experimental data and the solid curve *a* is the best fit of the algorithm incorporating PY^+, $(PY^+)_2$ and $\beta CD.PY^+$ to the chemical shift variations of protons H_1-H_5. Right ordinate: speciation relative to $[PY^+]_{total}$, curve *b* is the percentage of $[PY^+]$, curve *c* is twice the percentage of $[(PY^+)_2]$ and curve *d* is the percentage of $[\beta CD.PY^+]$.

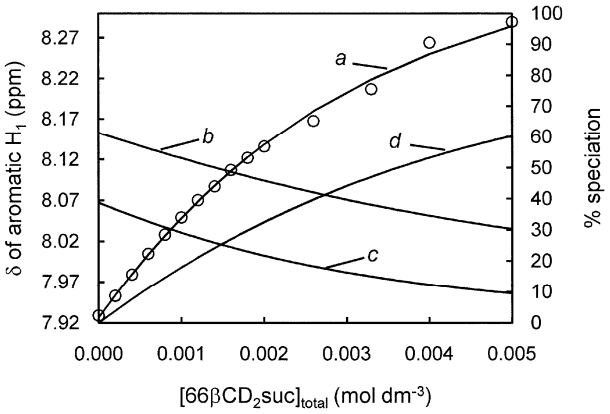

Fig. A53

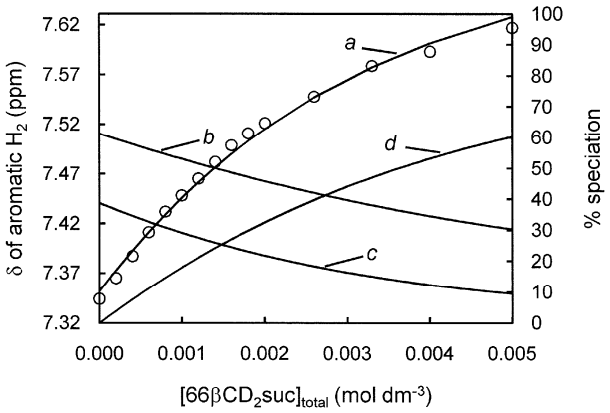

Fig. A54

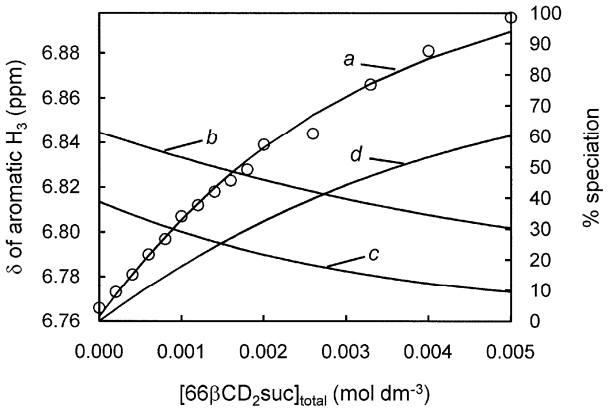

Fig. A55

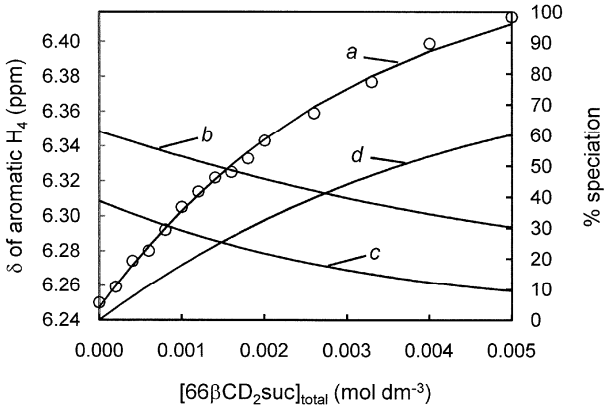

Fig. A56

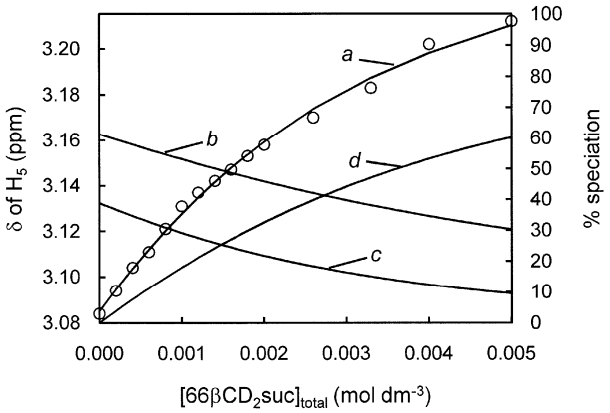

Fig. A57

Collective Caption for Figs. A53-A57. Left ordinate: variation of the ^{1}H (300 MHz) chemical shift of the aromatic H_1 proton (**Fig. A53**), aromatic H_2 proton (**Fig. A54**), aromatic H_3 proton (**Fig. A55**), aromatic H_4 proton (**Fig. A56**) and H_5 proton (**Fig. A57**) of PY^+ (2.00×10^{-3} mol dm^{-3}) with $[66\beta CD_2suc]_{total}$ (ranging from 0 to 5.00×10^{-3} mol dm^{-3}) in D_2O (1.00×10^{-4} mol dm^{-3} hydrochloric acid, I = 0.10 mol dm^{-3} NaCl) at 298.2 K. The circles are the experimental data and the solid curve *a* is the best fit of the algorithm incorporating PY^+, $(PY^+)_2$ and $66\beta CD_2suc.PY^+$ to the chemical shift variations of protons H_1-H_5. Right ordinate: speciation relative to $[PY^+]_{total}$, curve *b* is the percentage of $[PY^+]$, curve *c* is twice the percentage of $[(PY^+)_2]$ and curve *d* is the percentage of $[66\beta CD_2suc.PY^+]$.

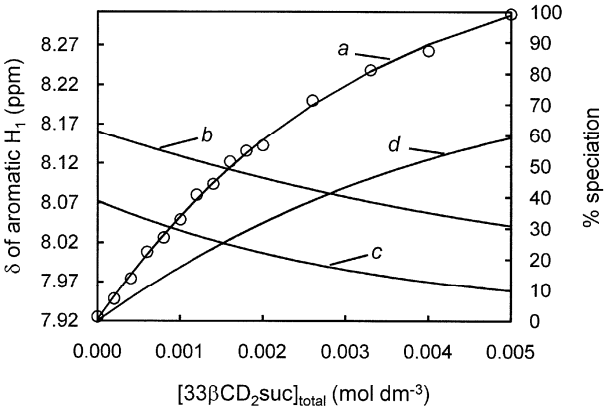

Fig. A58

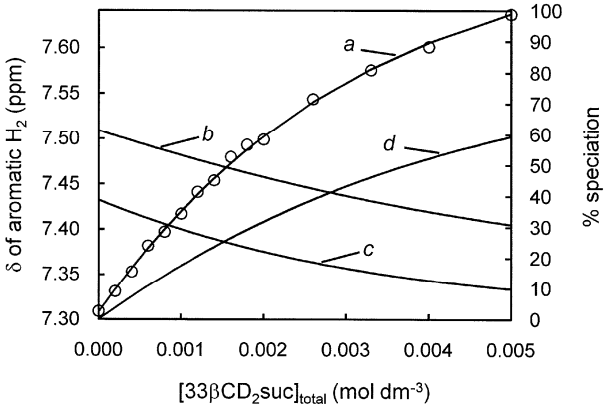

Fig. A59

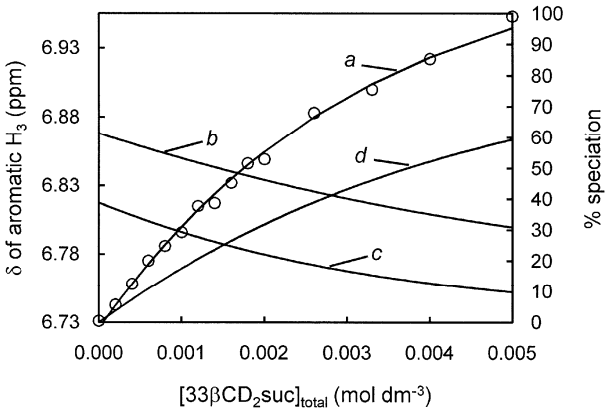

Fig. A60

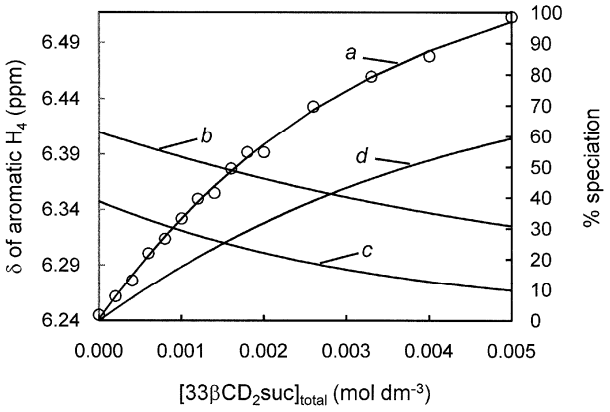

Fig. A61

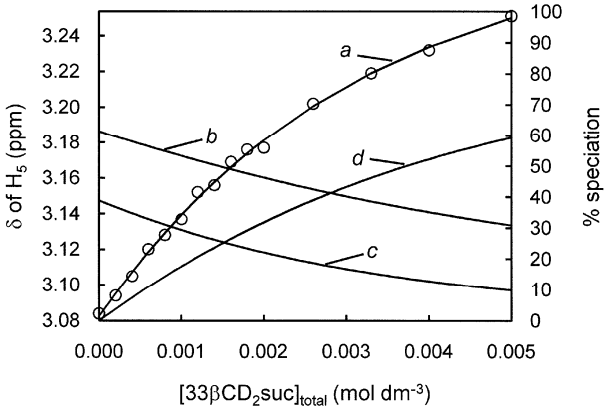

Fig. A62

Collective Caption for Figs. A58-A62. Left ordinate: variation of the ^{1}H (300 MHz) chemical shift of the aromatic H_1 proton (**Fig. A58**), aromatic H_2 proton (**Fig. A59**), aromatic H_3 proton (**Fig. A60**), aromatic H_4 proton (**Fig. A61**) and H_5 proton (**Fig. A62**) of PY^+ (2.00×10^{-3} mol dm^{-3}) with $[33\beta CD_2suc]_{total}$ (ranging from 0 to 5.00×10^{-3} mol dm^{-3}) in D_2O (1.00×10^{-4} mol dm^{-3} hydrochloric acid, I = 0.10 mol dm^{-3} NaCl) at 298.2 K. The circles are the experimental data and the solid curve *a* is the best fit of the algorithm incorporating PY^+, $(PY^+)_2$ and $33\beta CD_2suc.PY^+$ to the chemical shift variations of protons H_1-H_5. Right ordinate: speciation relative to $[PY^+]_{total}$, curve *b* is the percentage of $[PY^+]$, curve *c* is twice the percentage of $[(PY^+)_2]$ and curve *d* is the percentage of $[33\beta CD_2suc.PY^+]$.

^{1}H ROESY NMR Spectra

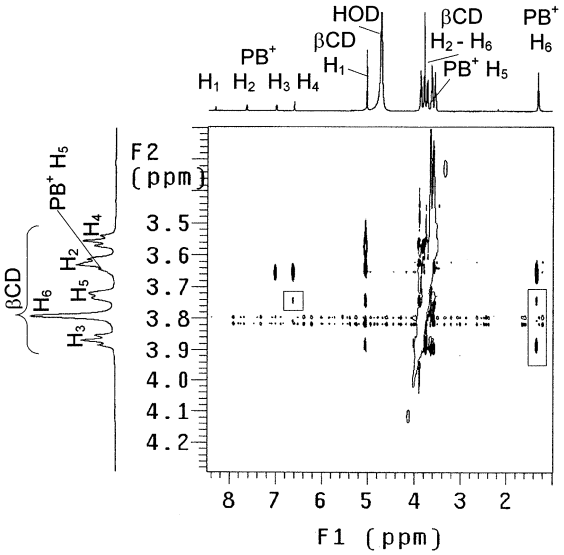

Fig. A63. 2D ^{1}H ROESY NMR (600 MHz) spectrum of PB^+ (2.0×10^{-3} mol dm^{-3}) with two molar equivalent βCD in D_2O (1.00×10^{-4} mol dm^{-3} hydrochloric acid, I = 0.10 mol dm^{-3} NaCl) at 298.2 K with a mixing time of 300 ms. Cross-peaks were observed between H_6 of PB^+ and H_3, H_5 of βCD; between aromatic H_4 of PB^+ and H_5 of βCD.

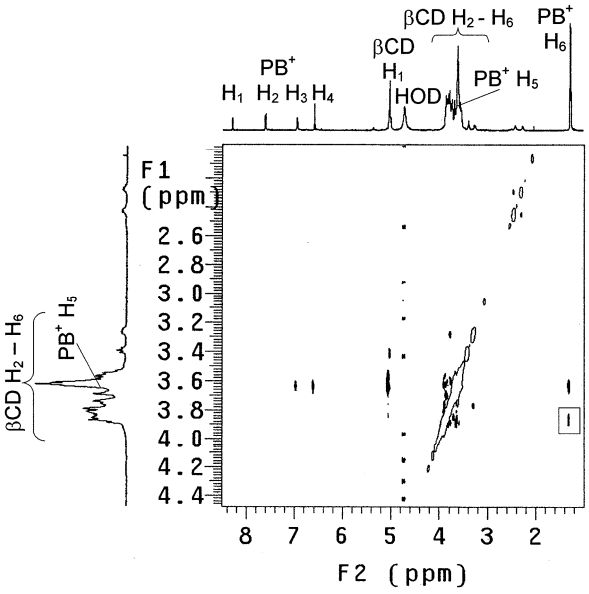

Fig. A64. 2D ^{1}H ROESY NMR (600 MHz) spectrum of PB^+ (2.0×10^{-3} mol dm^{-3}) and equimolar 66βCD$_2$suc in D_2O (1.00×10^{-4} mol dm^{-3} hydrochloric acid, I = 0.10 mol dm^{-3} NaCl) at 298.2 K with a mixing time of 300 ms. Cross-peaks were observed between H_6 of PB^+ and H_3-H_5 of βCD.

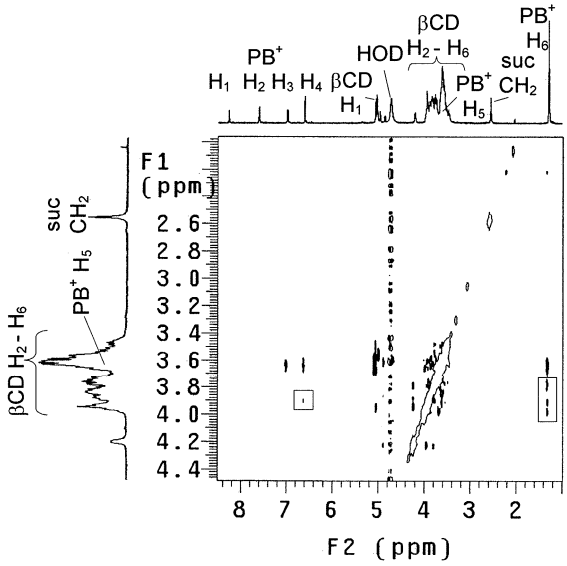

Fig. A65. 2D ^{1}H ROESY NMR (600 MHz) spectrum of PB^{+} (2.0×10^{-3} mol dm^{-3}) and equimolar 33βCD$_2$suc in D_2O (1.00×10^{-4} mol dm^{-3} hydrochloric acid, I = 0.10 mol dm^{-3} NaCl) at 298.2 K with a mixing time of 300 ms. Cross-peaks were observed between H_6 of PB^{+} and H_3-H_5 of βCD; between H_4 of PB^{+} and H_3-H_5 of βCD.

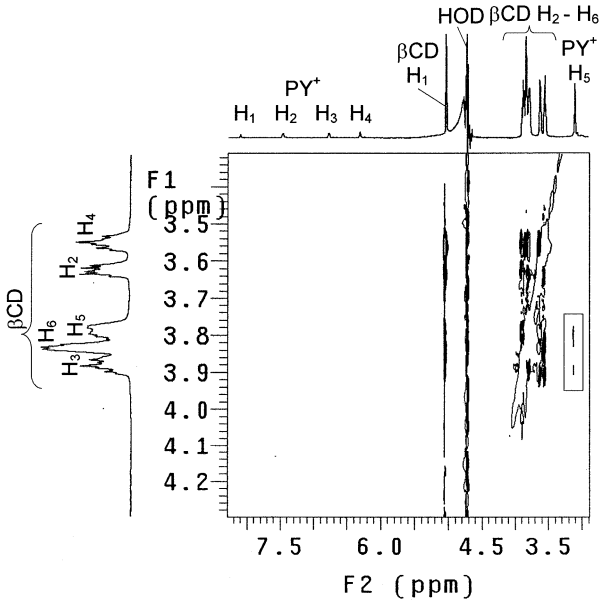

Fig. A66. 2D ^{1}H ROESY NMR (600 MHz) spectrum of PY^{+} (1.8×10^{-3} mol dm^{-3}) with two molar equivalent βCD in D_2O (1.00×10^{-4} mol dm^{-3} hydrochloric acid, I = 0.10 mol dm^{-3} NaCl) at 298.2 K with a mixing time of 300 ms. Cross-peaks were observed between H_5 of PY^{+} and H_3, H_5 of βCD.

Table A1. ^{1}H NMR Chemical shifts of PB^{+} and PY^{+} and their dimers and complexes of βCD, $33\beta CD_2suc$ and $66\beta CD_2suc$ derived from the fitting of appropriate equilibrium algorithms to chemical shift variation data in D_2O (1.00×10^{-4} mol dm^{-3} hydrochloric acid, I = 0.10 mol dm^{-3} NaCl at 298.2 K) as described in the main text..

Species	H_1 δ ppm	H_2 δ ppm	H_3 δ ppm	H_4 δ ppm	H_5 δ ppm	H_6 δ ppm
PB^{+}	8.334	7.680	7.108	6.822	3.657[a]	1.310[a]
$(PB^{+})_2$	7.0870	6.650	6.260	5.661	3.260[b]	1.059[b]
$\beta CD.PB^{+}$	8.508	7.786	7.114	6.722	N/A[c]	1.404
$33\beta CD_2suc.PB^{+}$	8.499	7.769	7.140	6.722	N/A[c]	1.397
$66\beta CD_2suc.PB^{+}$	8.524	7.772	7.098	6.713	N/A[c]	1.392
PY^{+}	8.305	7.630	7.039	6.654	3.238[a]	N/A[d]
$(PY^{+})_2$	7.332	6.809	6.327	5.600	2.904[b]	N/A[d]
$\beta CD.PY^{+}$	8.382	7.706	6.934	6.474	3.254	N/A[d]
$33\beta CD_2suc.PY^{+}$	8.516	7.815	7.062	6.652	3.335	N/A[d]
$66\beta CD_2suc.PY^{+}$	8.470	7.771	6.956	6.494	3.270	N/A[d]

δ referenced to external trimethylsilylpropiosulfonic acid in D_2O.

[a] Observed chemical shifts at the lowest concentration of $[PB^{+}]_{total}$ or $[PY^{+}]_{total}$
[b] Observed chemical shifts at the highest concentration of $[PB^{+}]_{total}$ or $[PY^{+}]_{total}$
[c] The H_5 proton resonance was not detectable due to overlapping with βCD signals
[d] The H_6 proton is not present in PY^{+}